Electronic Supplemental Information For:

An Acoustofluidic Trap and Transfer Approach for Organizing a High Density Single Cell Array

Korine A. Ohiri,[1,2] Sean T. Kelly,[1] Jeffrey D. Motschman,[1] Kevin H. Lin,[3] Kris C. Wood,[3] Benjamin B. Yellen[1,2,4,*]

1. Department of Mechanical Engineering and Materials Science, Duke University, Durham, NC 27708, USA
2. NSF Research Triangle Materials Research Science and Engineering Center, Duke University, Durham, NC 27708, USA
3. Department of Pharmacology and Cancer Biology, Duke University, Durham, NC 27708, USA
4. Department of Biomedical Engineering, Duke University, Durham, NC 27708, USA

***Corresponding Author:** *E-mail:* yellen@duke.edu

Submitted to: *Lab on a Chip*

Key terms: single cell isolation, high throughput, bulk acoustic waves, lab-on-a-chip, microfluidics, acoustofluidics

1. Alternative Microfluidic Designs

A high density acoustofluidic array (i.e. ≈12 cmpts/mm^2) with a footprint of 25 x 75 mm consisting of 8 sections of 20 compact acoustofluidic elements in series and 32 elements in parallel (e.g. > 5000 compartments total) was tested (Figure S1). Here, the vertical length from the top of the compartment region to the first bend in the bypass channel (Figure S1, solid line) is 255 µm while the length to the bottom of the bypass is 470 µm (Figure S1, dashed line). We additionally observed successful acoustic transfer across a broad range of frequencies, ranging from 2.7 to 2.9 MHz.

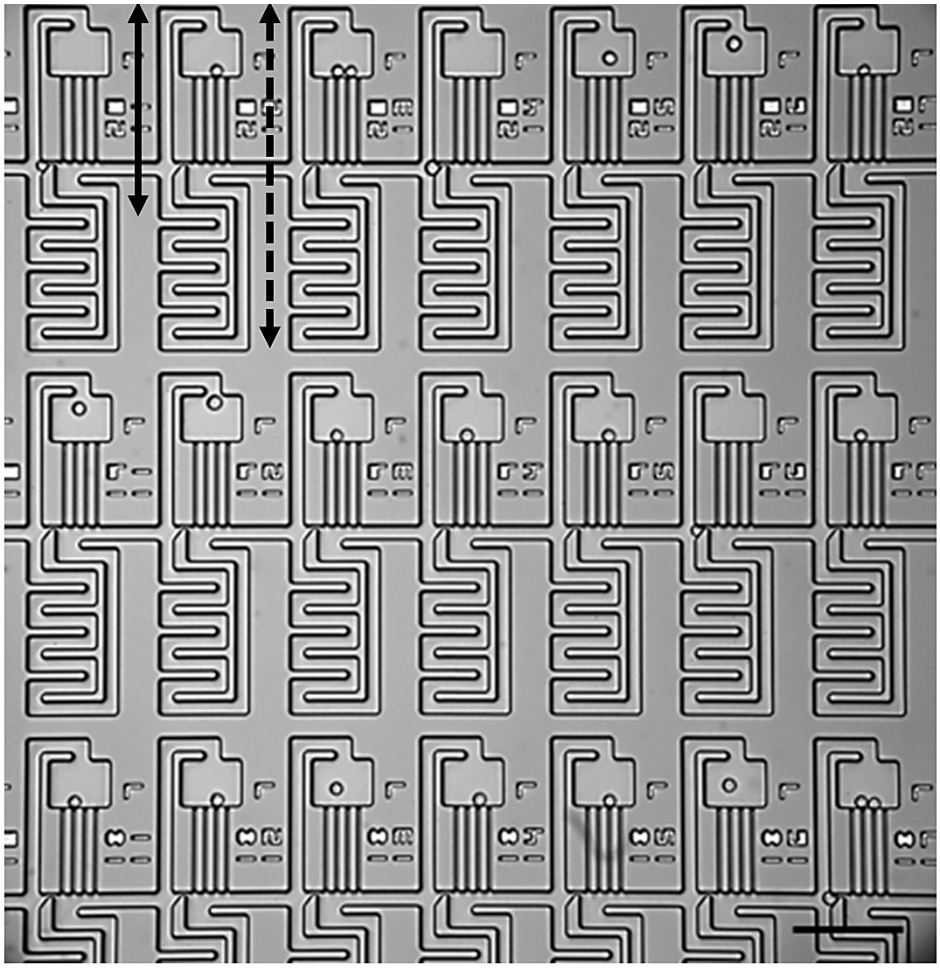

Figure S1. Single cell array generated in high density chip excited at 2.9 MHz and 16 V_{pp}. Solid line indicates distance from top of compartment region to the first bend of the bypass channel (i.e. 255 µm) while the dashed line indicates the distance from the compartment region to the bottom of the bypass (i.e. 470 µm). Scale bar is 200 µm.

2. Shear Stress Through the Acoustofluidic Element

As an upper bound of the fluidic shear applied to the trapped cells, we used COMSOL Multiphysics to calculate the flow distribution through an unoccupied weir, from which the shear stress can be calculated (Figure S2(a)).

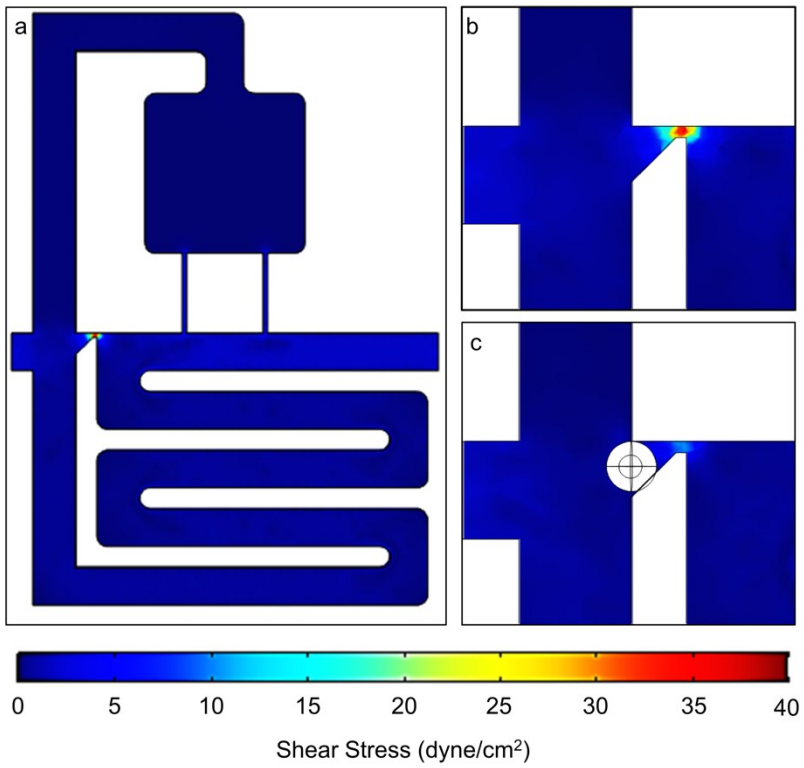

Figure S2. Shear stress in (a) an acoustofluidic element, (b) unoccupied weir site, and (c) occupied weir site assuming an inlet pressure of 20 mbar (i.e. a pressure drop of ~0.5 mbar per weir).

To corroborate this result, we also estimated the shear stress from the analytical solution of parabolic flow in between two parallel plates,[1] which yields

$$\tau = \frac{6\eta Q}{h^2 w} \tag{S1}$$

where η is the dynamic viscosity, Q is the volumetric flow rate, h is the height of the weir, and w is the width of the weir. The volumetric flow rate through the weir site of an acoustofluidic element can be calculated by dividing the pressure drop across one array period (i.e. ~0.5 mbar per weir) by the resistance through the region. Here, we calculated the pressure drop across an

individual acoustofluidic element by dividing the inlet pressure (i.e. 20 mbar) by the number of traps in series. Thus, in both the COMSOL calculations and the analytical model, the fluid shear stress through the weir site was 20-40 dyne/cm^2 (Figure S2(b)). We note that this estimate is an upper bound, since the presence of a cell will disturb the flow profile through the trap and decrease the shear significantly (Figure S2(c)). Additionally, the cells are only temporarily placed in the weirs sites (e.g. < 30 minutes) and are switched to compartment regions with significantly lower shear (e.g. < 0.4 dyne/cm^2).

3. Material Dependence of Acoustic Radiation Force

In a standing acoustic wave, the acoustic radiation force (F^{rad}) exerted on a spherical particle suspended in a viscous fluid is described by:[2]

$$F^{rad} = -\nabla U^{rad}, \tag{S2.a}$$

$$U^{rad} = \frac{4\pi}{3}a^3\left[\frac{f_1}{2}\kappa_0\langle p_{in}^2\rangle - \frac{3Re[f_2]}{4}\rho_0\langle v_{in}^2\rangle\right], \tag{S2.b}$$

$$f_1 = 1 - \frac{\kappa_p}{\kappa_0}, \tag{S2.c}$$

$$f_2 = \frac{2(1-\Gamma)(\rho_p - \rho_0)}{2\rho_p + \rho_0(1-3\Gamma)}. \tag{S2.d}$$

Where U^{rad} is the radiation potential, f_1 is the monopole coefficient, κ_0 and κ_p are the compressibilities of the fluid and particle respectively, f_2 is the dipole coefficient, ρ_0 and ρ_p are the densities of the fluid and particle respectively, and Γ is a complex system dependent parameter that is a function of the viscous penetration depth. Thus, due to contributions from the monopole and dipole coefficient, the relative material properties of the particle or cell in suspension dictate their preferred position in the acoustic energy landscape. While a positive monopole coefficient or negative dipole coefficient can cause particles in suspension to migrate to the pressure node, a negative monopole coefficient or positive dipole coefficient can cause particles to migrate to the pressure antinode. Typically, in one-dimensional systems these two coefficients are combined and referred to as the acoustic contrast factor.[3, 4] Although this acoustic contrast factor is an over-simplification of the two-dimensional migration observed in

these studies, the basic concept remains that particles with negative (positive) acoustic contrast factor should move to the time averaged pressure maxima (minima) respectively.

For our purposes, both the observed engineered PDMS-based microparticles (NACPs) and cells are nearly neutrally buoyant with the surrounding fluid, having relative densities ranging from approximately 0.9 to 1.1.[4, 5] Thus, contributions from the monopole coefficient dominate. NACPs are more compressible than the suspending fluid and exhibit a negative monopole coefficient, whereas cells are less compressible than cell media and thus exhibit a positive monopole coefficient. Thus, if migration were due to the acoustic radiation force, we would expect that NACPs and cells would be driven to different locations in the energy landscape.[6, 7] However, in our device both the NACPs and PC9s focus to the same location (Figure S3), indicating that switching is not due to an acoustic radiation force, and instead caused by steady acoustic streaming.

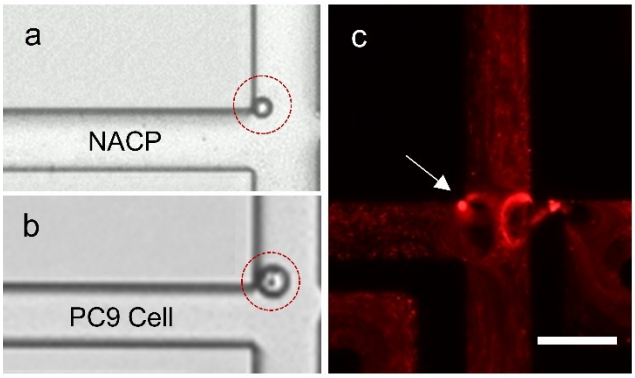

Figure S3. Acoustic switching of NACPs and PC9 cells. (a) Capture of a NACP on the leading corner of the compartment region. (b) Capture of a PC9 cell in the same location on the leading corner of the compartment region. (c) Zoom-in of streaming patterns in the trifurcation region for 300 nm red PS beads upon acoustic excitation at 1.4 MHz and 16 V_{pp}. Scale bar indicates 50 μm.

4. Fabrication Routine for the Acoustofluidic Chips

Figure S4 below details a general flow chart for the fabrication routines for the acoustofluidic chips. There are two general processes; one that results in chips with topside access ports via holes drilled in the glass lid and one that results in chips with backside access ports by etching through holes in the silicon. We note here that while both processes are similar, Figure S4(d-e) are optional steps to generate backside access ports and are not required for

topside access. However, for topside access, the glass lid must have inlet and access ports pre-drilled before sealing the microfluidic chip and individual chips must be manually separated from the wafer.

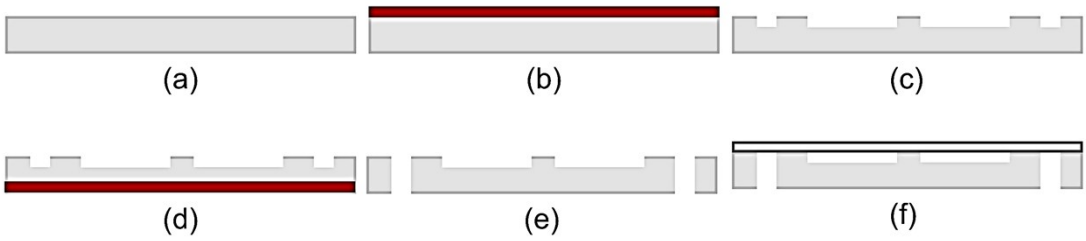

Figure S4. Flow chart for fabrication of acoustofluidic chips. (a) A bare silicon wafer is selected and cleaned. (b) The pattern for the microfluidic devices are transferred to the front side of the wafer using photolithography. (c) The pattern for the microfluidic devices is etched into the front side of the silicon using deep reactive ion etching. (d) Through holes are patterned onto the backside of the wafer using photolithography. (e) Through holes are etched into the backside of the water using deep reactive ion etching and the individual chips are separated from the wafer. (f) The microfluidic chips are sealed with a glass lid using anodic bonding. Here, gray represents silicon, red represents photoresist, and white represents glass.

5. Acoustofluidic Assembly with Backside Access Ports

The alternative configuration for the acoustofluidic assembly has backside access ports (Figure S5). In combination with a custom 3D printed stage, this configuration enables facile imaging with an inverted microscope.

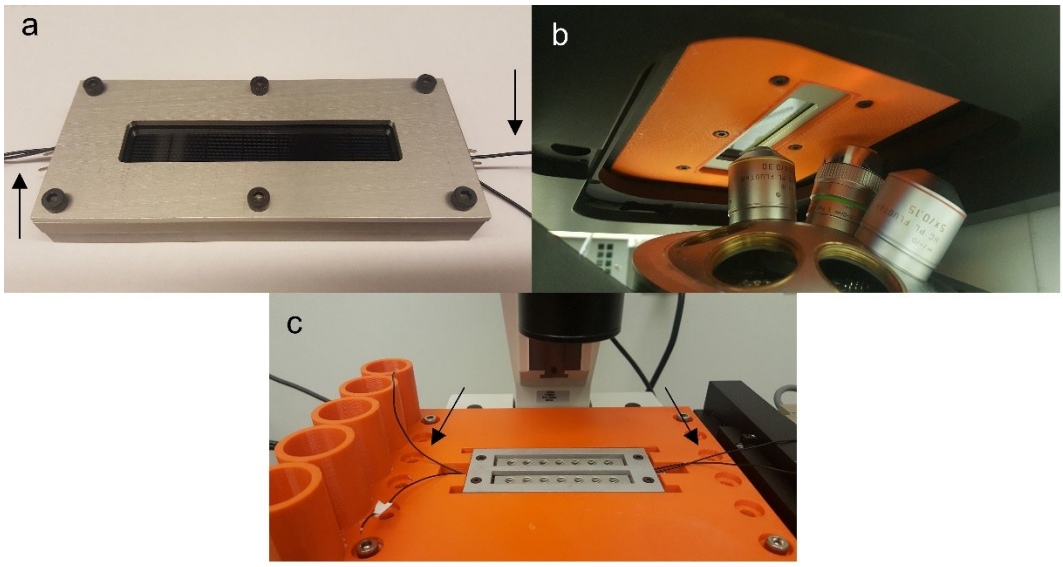

Figure S5. Various configurations of acoustofluidic assembly with backside access ports. (a) Acoustofluidic chip in aluminum manifold. (b) Top view of acoustofluidic assembly in custom stage for inverted microscope. (c) Bottom view of acoustofluidic assembly in custom stage for inverted microscope. Arrows indicate leads to piezoelectric transducers.

6. Movie Captions

Movie 1: Loading of 8.5 µm polystyrene beads. Beads are withdrawn from weir sites in the acoustofludic element then propelled forwards with acoustics turned off. As can be seen, the bead that does not enter the weir site alternatively travels along the bypass.

Movie 2: Trap and transfer of 8.5 µm polystyrene beads. At the start of the video, beads are loaded in weir sites and subsequently manually (i.e. via syringe) transferred into adjacent compartment regions for demonstration purposes in the remainder of the video. First, beads are withdrawn and pumped from and to weir sites at a low speed (i.e. < 100 µm/s) to ensure particle doublets were not present. Next, beads are again withdrawn from weir sites for < 3 seconds at a low speed such that they do not pass the outlets of the compartment regions. Immediately prior to reversing the fluid flow, the acoustic signal is turned on (i.e. with a frequency sweep from 1.35 to 1.42 MHz at a rate of 1 Hz and excitation of 5 V_{pp}) and beads are pumped forward at a low speed. Following capture at the leading corner of the compartment region, the acoustic signal is turned off and beads are pumped into the compartment region. Move is shown in real time.

Movie 3: Particle motion of 200 nm polystyrene beads upon no acoustic excitation and excitation at 14.6 V_{pp}, 17 V_{pp}, and 19.2 V_{pp}. A suspension of 200 nm polystyrene beads was injected into the microfluidic chip using an Elveflow pressure controllers. Once filled, forward pressure was turned off and while the acoustic signal was still off a movie was recorded for the 0 V_{pp} condition. Subsequently, while forward pressure was still off the acoustic signal was turned on (i.e. with a frequency of 1.4 MHz) and movies were recorded at excitations of 14.6 V_{pp}, 17 V_{pp}, and 19.2 V_{pp}, which show the streaming vortices near the sharp corners.

Movie 4: Trap and transfer of PC9 cancer cells. At the start of the video, PC9 cells are loaded in weir sites and subsequently manually (i.e. via syringe) transferred into adjacent compartment regions for demonstration purposes in the remainder of the video. First, cells are withdrawn and pumped from and to weir sites at a low speed (i.e. < 50 μm/s) to ensure doublets were not present. While cells are being pumped forwards at a low speed, the acoustic signal was turned on (frequency sweep from 1.35 to 1.42 MHz at a rate of 1 Hz and excitation of 16 V_{pp}). After cells were captured at the leading corner of the compartment region, the acoustic signal was turned off and positive pressure was applied to transfer cells into the compartment region. The process is repeated once more to capture most of the remaining cells. Move is shown in real time.

References

1. L. Kim, M. D. Vahey, H. Y. Lee and J. Voldman, *Lab Chip*, 2006, **6**, 394-406.
2. P. B. Muller, R. Barnkob, M. J. Jensen and H. Bruus, *Lab Chip*, 2012, **12**, 4617-4627.
3. K. A. Ohiri, B. A. Evans, C. W. Shields IV, R. A. Gutiérrez, N. J. Carroll, B. B. Yellen and G. P. López, *ACS applied materials & interfaces*, 2016, **8**, 25030-25035.
4. C. W. Shields, D. Sun, K. A. Johnson, K. A. Duval, A. V. Rodriguez, L. Gao, P. A. Dayton and G. P. López, *Angewandte Chemie International Edition*, 2014, **53**, 8070-8073.
5. W. H. Grover, A. K. Bryan, M. Diez-Silva, S. Suresh, J. M. Higgins and S. R. Manalis, *Proc Natl Acad Sci U S A*, 2011, **108**, 10992-10996.
6. M. Settnes and H. Bruus, *Phys Rev E Stat Nonlin Soft Matter Phys*, 2012, **85**, 016327.
7. I. Leibacher, P. Hahn and J. Dual, *Microfluidics and Nanofluidics*, 2015, **19**, 923-933.